RSC Applied Polymers

PAPER

View Article Online
View Journal | View Issue

Cite this: *RSC Appl. Polym.*, 2026, **4**, 753

Enhancing the mechanical properties of epoxy with graphene quantum dots: a molecular dynamics study

Swapnil S. Bamane, *[a] Prathamesh P. Deshpande, [b] Folarin Erogbogbo[c] and Ozgur Keles [a]

Polymers are the key to the next generation of high-performance materials for their applications in aerospace, defense, and energy. Thermoset polymers like epoxy are widely used as a matrix material in composites due to their ease of processability and compatibility with reinforcement materials. There have been significant efforts in the development of polymer materials properties using nanofillers such as graphene, carbon nanotubes, rubber, and metal oxides. However, graphene quantum dots (GQD), a zero-dimensional nano-scale filler material, have not been extensively explored towards improvement of the mechanical properties of polymers. The objective of this study is to understand the effects of GQDs on the mechanical properties of the epoxy. The impact of various functional GQDs is evaluated on mechanical properties such as Young's Modulus, yield strength, and Poisson's ratio. The predicted materials properties using a fixed-bond interface forcefield (IFF) are compared with a reactive forcefield, ReaxFF. The results of this study demonstrate that the amine-functionalized GQDs improve the Young's modulus of the epoxy by 14% and the yield strength by 47%. Furthermore, MD simulations offer nanoscale insights into the energy distributions, free volume, and increase of free volume pockets in the material. The results and observations of this study provide valuable nano-scale insights into accurate and efficient modeling of GQD nanocomposite materials for high-performance applications in aerospace, defense, and energy.

Received 24th November 2025,
Accepted 23rd January 2026

DOI: 10.1039/d5lp00373c

rsc.li/rscapplpolym

1. Introduction

In recent years, polymer matrix composite (PMC) materials have been of interest in the aerospace domain as a primary structural material due to their high strength-to-weight ratio. The favored reinforcement materials are carbon structures, such as graphene, carbon nanotubes (CNTs), and flattened CNTs (flCNTs), which exhibit exceptional mechanical strength, such as a Young's Modulus of 1 TPa and a tensile strength of 11–63 GPa.[1,2] These outstanding properties are inherently unidirectional or confined to a single plane due to the anisotropic nature of the nanostructures. Typically, composite laminates are synthesized using a polymer matrix to achieve orthotropic or quasi-isotropic properties. However, the mechanical properties of the resulting composite materials are inferior[3,4] compared to pristine reinforcement materials due to the weaker matrix and an interface that lowers the performance of the composite materials.[5]

Both thermoset and thermoplastic polymers, such as epoxy, PEEK, and polyimides, are commonly used as matrix materials. Specifically, epoxies have been extensively used as a matrix material due to their ease of processing.[6–16] Epoxy typically shows a Young's modulus ranging between 2.5–3.0 GPa and a tensile strength of 55–90 MPa.[15,17,18] Compared to carbon reinforcement materials, the mechanical properties of the epoxy are significantly lower. Enhancements in the mechanical properties of the neat epoxy resin will improve the overall performance of the composite. Therefore, to develop next generation high-performance composite materials, it is important to improve the baseline properties of neat epoxy as a matrix.

Numerous studies have demonstrated that the use of traditional nanofiller materials, such as graphene, fullerene, and CNTs, enhances the mechanical properties of the epoxy.[22–24] Table 1 shows the mechanical properties of the neat bisphenol F epoxy and nanofiller-enhanced epoxy nanocomposites. Table 1 shows that the improvements in the mechanical properties of the epoxy depend on the nanofiller material, reinforcement mass fraction, the type of functionalization, and the strain rate applied during mechanical testing. Specifically, functional groups such as amines and oxides provide

[a]*Department of Mechanical Engineering and Engineering Science, University of North Carolina at Charlotte, Charlotte, NC 28223, USA. E-mail: sbamane@charlotte.edu*
[b]*Department of Metallurgy and Materials Engineering, COEP Technological University, Pune, Maharashtra 411005, India*
[c]*Department of Biomedical Engineering, San Jose State University, San Jose, CA 95192, USA*

Table 1 Experimentally measured mechanical properties of neat bisphenol F epoxy and epoxy nanocomposites with graphene-based nanofillers

Material	Reinforcement mass fraction (wt%)	Young's modulus (GPa)	Tensile strength (MPa)	Strain rate (s^{-1})	Ref.
Epoxy	0	2.5	58	0.00001	15
Epoxy	0	2.8	65	0.001	15
Epoxy	0	2.95	82	0.1	15
Epoxy	0	1.6	60	0.0001	18
Epoxy	0	2.25	80	1	18
Epoxy	0	3.2	85	1000	18
Epoxy-graphene	0.5	2.95 ± 0.10	NA	0.05	19
Epoxy-graphene	1	3.05 ± 0.05	NA	0.05	19
Epoxy-graphene oxide	0.1	3.3 ± 0.8	70 ± 1	2 mm min^{-1} [a]	20
Epoxy-graphene oxide	0.25	3.15 ± 1	70 ± 3	2 mm min^{-1} [a]	20
Epoxy-graphene oxide	0.5	3.15 ± 0.5	75 ± 3	2 mm min^{-1} [a]	20
Epoxy-NH_2-graphene	0.5	2.7	78	NA	21
Epoxy-NH_2-graphene	1	2.75	60	NA	21

[a] Rate of displacement is mentioned instead of strain rate. NA – not available.

increased interactions through covalent bonding, hydrogen bonding, and coulombic attractions, affecting the mechanical properties of the epoxy.

However, these improvements in the mechanical properties are limited due to processing-induced defects, such as lower crosslinking density, void formation, and increased free volume near the nanofiller region. These interfacial defects act as crack nucleation sites and cause delamination. These drawbacks are dependent on the size of the nanofillers used in the epoxy nanocomposites. The typical sizes of nanofillers are 10–20 μm for clay nanofillers,[24,25] 30–90 nm for rubber particulates,[26,27] 6–140 nm in diameter for CNTs,[28,29] and 1–50 μm for graphene platelets.[30] There is a possibility of controlling the defect sizes and free volume by introducing a relatively smaller-sized nanofiller element. Therefore, there is a need to explore nanoparticles that alleviate the formation of interfacial defects and strengthen the epoxy matrix.

Deshpande *et al.*[31,32] demonstrated that graphene quantum dot (GQD) nanofillers improve the mechanical properties of the epoxy. GQDs provide a platform to control the surface chemistry of the filler. Therefore, GQDs can be tailored to enhance the interfacial interaction with epoxy or other polymer systems. In addition, GQDs' size, number of layers, and edge structures can be adjusted *via* synthesis conditions.[33,34] Molecular dynamics (MD) simulations predicted an overall increase of 7% in the stiffness and a 33% increase in the yield strength of bisphenol F epoxy using ReaxFF, a reactive force field. ReaxFF is a popular MD force field and has been used extensively to predict the material properties of various materials due to its ability to form and dissociate bonds based on Pauling's concept of bond order potential.[35] However, ReaxFF is computationally demanding compared to a fixed bond force field, thus limiting the size of a simulation.[36] Larger MD simulations are better positioned to reveal the effects of long-range GQD interactions, multiple GQDs, and the mass fraction of GQDs on the matrix properties. Thus, for accelerated and accurate computational research in the domain of QDs, there is a need to investigate their interactions using MD simulations with a computationally efficient and accurate force field designed for interfaces.

The Interface Force Field (IFF) has previously been used to predict the thermo-mechanical properties of the polymers.[12,37–43] The IFF is a fixed-bond force field with the capability of chemical reaction modeling.[36] IFF is computationally efficient compared to ReaxFF.[36] Winetrout *et al.*[36] demonstrated that for single-wall carbon nanotubes (SWCNTs), polyacrylonitrile (PAN), cellulose Iβ, and γ-iron, ReaxFF overpredicted the mechanical properties compared to experimentally measured properties. IFF has previously been used to model flattened CNTs (flCNTs),[44] CNTs,[38] boron nitride nanotubes (BNNTs),[39,40] and various polymers.[38,44,45]

Bamane *et al.*[46] recently modeled GQDs using IFF and demonstrated improved thermal stability of epoxy. However, GQDs have not yet been simulated for the prediction of mechanical properties using IFF parameters. There is a need to simulate GQD–epoxy nanocomposites using IFF parameters for mechanical property predictions with efficient and accelerated computational research.

The objective of this study is to investigate the effects of GQDs on the mechanical properties of the epoxy using MD. The MD predicted material properties using IFF parameters are compared with the mechanical properties predicted by Keles *et al.*[32] and Deshpande *et al.*[31] using ReaxFF parameters.[47] The nanoscale mechanisms behind the effects of GQDs on the material properties and the effects of free volume on the mechanical properties are discussed. Furthermore, interfacial interactions and the effects of functionalization of GQDs on the mechanical properties of epoxy are investigated. The predictions made in this study are important for further material discovery in the field of GQD-based nanocomposite materials for their application in aerospace and defense.

2. MD modeling

MD simulations were performed using the Large-scale Atomic/Molecular Massively Parallel Simulator (LAMMPS)[48] software

package developed by Sandia National Laboratory. All-atom MD models were utilized to simulate the GQD–epoxy nanocomposite materials modeled herein. The forcefield parameters were imported from a class-2, fixed bond forcefield, IFF developed by Heinz *et al.*[49] LAMMPS Utility for Network Analysis and Reactivity (LUNAR)[50] was utilized to postprocess the MD-generated data. OVITO,[51] a visualization tool, was used to create the snapshots of the MD models.

2.1. MD modeling of GQDs

The GQD MD model was created in AVOGADRO.[52] The GQD model was hexagonal in shape with a size of ~1.8 nm in diameter. GQD models consisted of a total of 90 carbon atoms. The valency of edge carbon atoms in GQDs was terminated using hydrogen atoms. A total of 9 GQD models were created with various functional groups attached to GQDs at random locations for interfacial crosslinking. IFF has successfully been used to model sp^2 carbon structures such as CNTs[38] and flCNTs.[44,53] Similarly, GQDs are sp^2 carbon structures, essentially a zero-dimensional form of graphene with a size of 1–20 nm in diameter.[54] Furthermore, previous MD simulation studies involved GQD models with ReaxFF and IFF parameters.[31,32,46] Therefore, GQDs can effectively be modeled using IFF parameters in MD simulations. Below are the details of each GQD model created.

1. Pristine GQD: A pristine GQD model consisted of 120 total atoms, including 90 carbon and 30 edge hydrogen atoms. This is referred to as GQD hereafter. Fig. 1(a) shows the molecular structure of the GQD model.

2. e4N-GQD: The e4N-GQD model was functionalized with a primary amine group at 4 unique randomly selected edge locations. Fig. 1(b) shows the molecular structure of the GQD model.

3. e6N-GQD: Similar to e4N-GQD, a total of six primary amine groups were attached to the e6N-GQD model as shown in the molecular structure in Fig. 1(c).

4. s4OH-GQD: The s4OH-GQD model was created by attaching four hydroxyl groups on randomly selected sites on the surface of GQD. The molecular structure of s4OH-GQD is shown in Fig. 2(a).

5. s8OH-GQD: Similar to s4OH-GQD, a total of eight hydroxyl groups were attached to the GQD surface, as shown in Fig. 2(b).

6. s4OH-e4OH-GQD: The s4OH-e4OH-GQD model was created by attaching four hydroxyl groups on the surface and four hydroxyl groups on the edge of the GQD. The functional sites on both the surface and edge were randomly selected. Fig. 2(c) shows the molecular structure of the s4OH-e4OH-GQD.

7. s4O-GQD: The s4O-GQD model was created by attaching four epoxide groups on randomly selected sites on the surface of the GQD. The molecular structure of s4O-GQD is shown in Fig. 3(a).

8. e4COOH-GQD: The e4COOH-GQD model was created by attaching four carboxyl functional groups on randomly selected edge sites on the GQD. The molecular structure of s4O-GQD is shown in Fig. 3(b).

9. e4COOH-s4O-GQD: The e4COOH-s4O-GQD model was created by attaching four carboxyl groups on the edge and four epoxide groups on the surface of the GQD. The functional sites on both the surface and edge were randomly selected. Fig. 3(c) shows the molecular structure of the e4COOH-s4O-GQD.

2.2. MD modeling of the epoxy nanocomposite

Diglycidyl ether of bisphenol F (DGEBF) epoxy resin and diethyl toluene diamine (DETDA) hardener were modeled with a stochiometric ratio of resin : hardener as 2 : 1. This epoxy system is modeled after EPON 862-DETDA epoxy. Fig. 3(d) and (e) show the molecular structure of DGEBF and DETDA, respectively. The input LAMMPS data files of the monomers for DGEBF and DETDA were created using IFF parameters. The

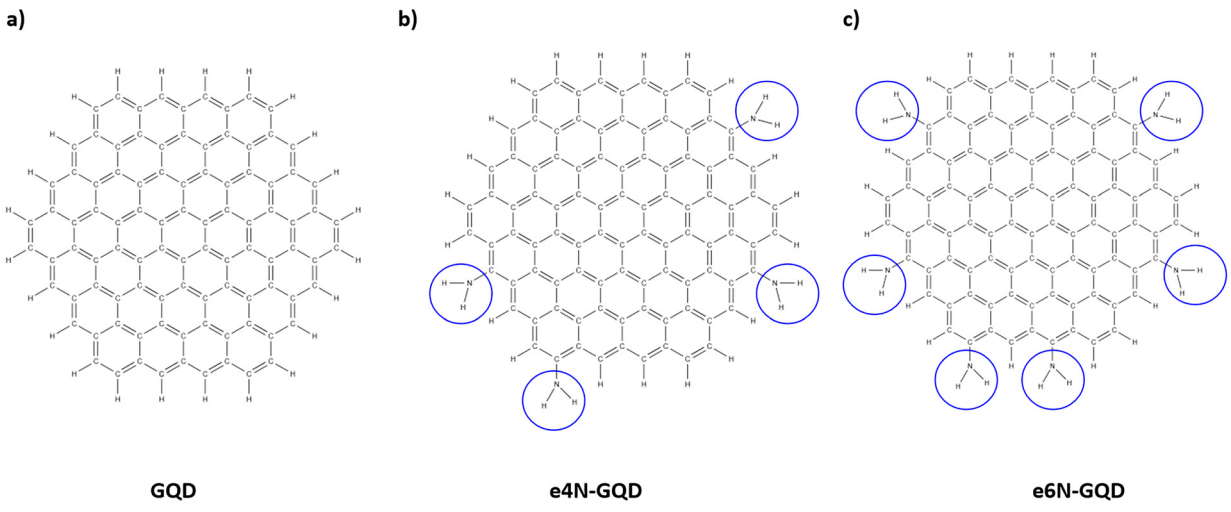

Fig. 1 Molecular structures of (a) pristine GQD, (b) e4N-GQD, and (c) e6N-GQD. The blue circles highlight the amine functional group sites.

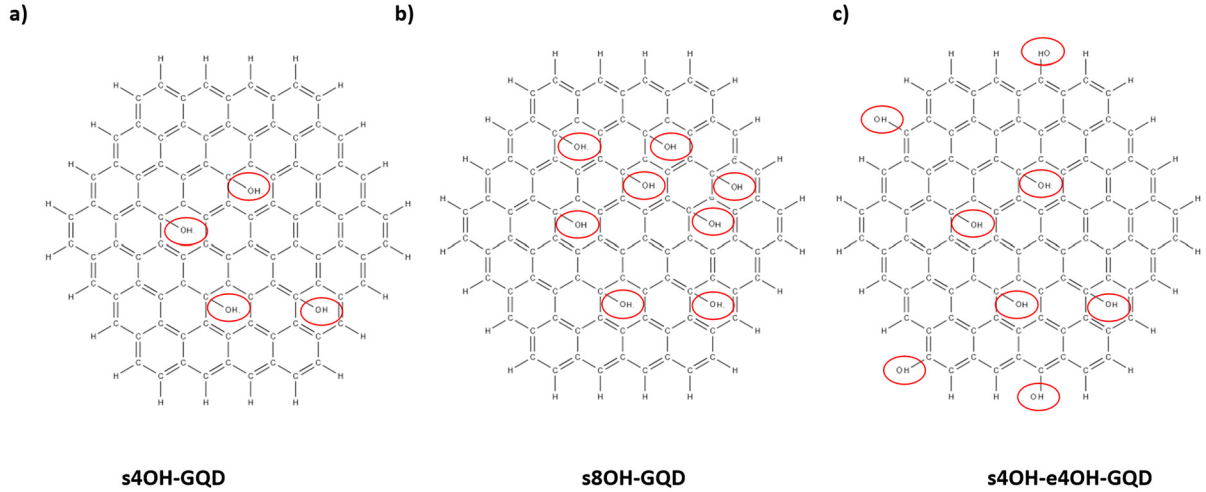

Fig. 2 Molecular structures of GQDs functionalized with hydroxyl groups illustrating (a) s4OH-GQD, (b) s8OH-GQD, and (c) s4OH-e4OH-GQD. The red circles highlight the hydroxyl functional group sites.

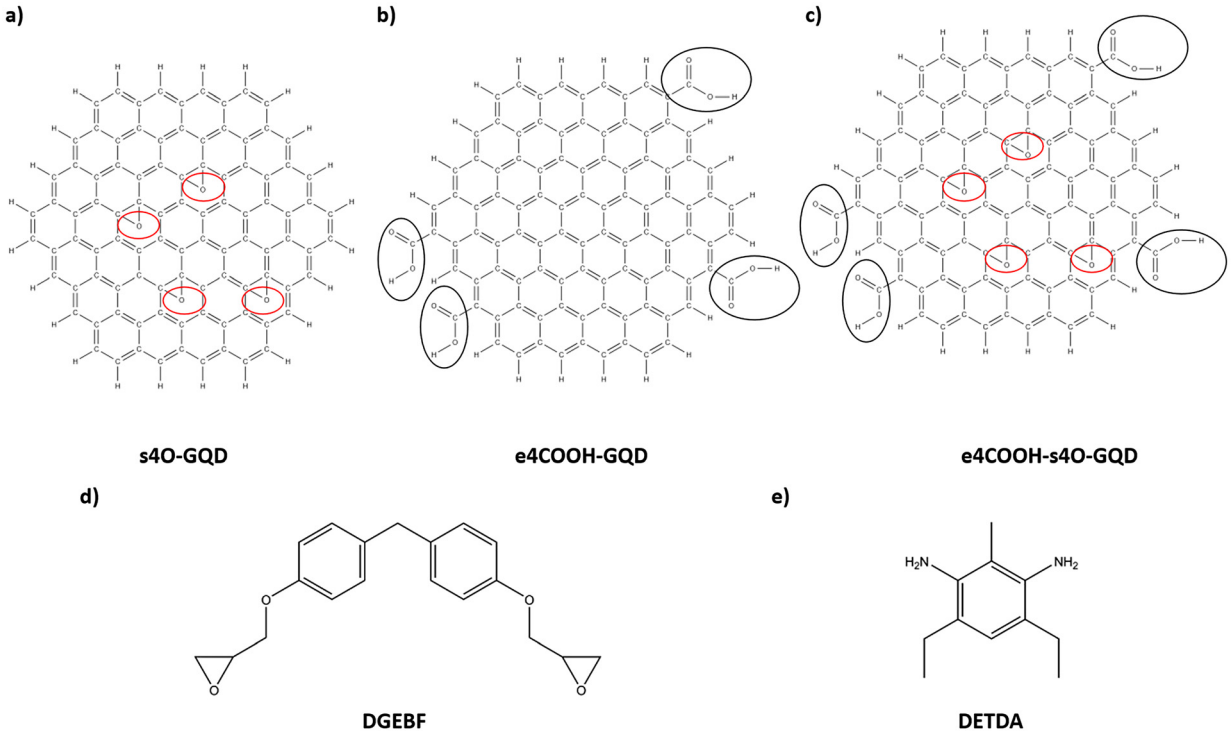

Fig. 3 Molecular structures of GQDs with epoxide and carboxyl functional groups illustrating (a) s4O-GQD, (b) e4COOH-GQD, (c) e4COOH-s4O-GQD, (d) DGEBF, and (e) DETDA. The red circles highlight the epoxide functional group sites and the black circles highlight the carboxyl functional group sites.

atomic positions were generated using ChemDraw.[55] Energy minimization was performed for the monomer data files in LAMMPS using the conjugate gradient method in LAMMPS. Fig. 4(a) illustrates the MD models of DGEBF resin and DETDA hardener.

The epoxy monomers were imported into a periodic simulation box in all three *x*-, *y*-, and *z*-directions and were replicated to create a bulk polymer system. A total of 96 resin molecules and 48 hardener molecules were created. A total of 5616 atoms were modeled to simulate epoxy. The GQD model, as shown in Fig. 4(b), was inserted into the epoxy model at this stage. For neat epoxy models, the mixing step was eliminated. The GQD wt% in the nanocomposite models was 3.1%. The number of atoms and the GQD wt% were kept similar to the

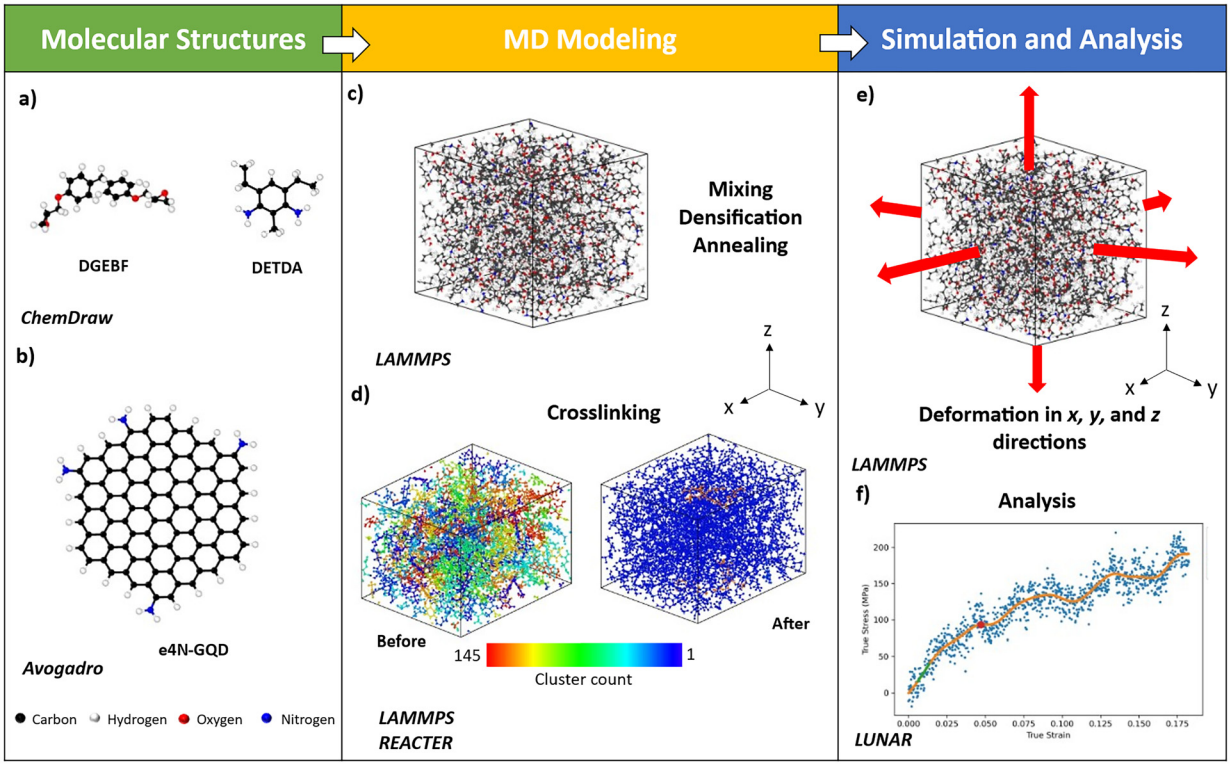

Fig. 4 MD framework demonstrating (a) snapshot of DGEBF and DETDA MD model, (b) snapshot of the e4N-GQD MD model, (c) snapshot of an epoxy nanocomposite MD model after densification, (d) cluster analysis performed in OVITO to illustrate crosslinking, (e) illustration of mechanical test simulations, and (f) representative stress–strain plot generated using LUNAR to predict mechanical properties.

ReaxFF models developed by Deshpande *et al.*[31] for direct comparison of the results between the two forcefields.

The densification simulations were performed, where models were densified to the target density of 1.17 g cc^{-1} at 300 K in a controlled volume and temperature (NVT) ensemble. The target density for densification simulation is selected lower than the experimentally reported mass density of 1.2 g cc^{-1} (ref. 17) to simulate monomers. The uncured density of epoxy is reported as ranging from 1.14–1.18 g cc^{-1}.[56] The value of 1.17 g cc^{-1} is typical in MD simulations as a target density to simulate an uncured bisphenol-F epoxy system.[17,31,42,46,57,58] The 1-step densification was performed using the "fix deform" command in LAMMPS, where the simulation box was deformed from an initial density of 0.20–0.22 g cc^{-1} to the target density uniformly in all three *x*-, *y*-, and *z*-directions at a constant strain rate of 10^{-6} Å fs^{-1}. For densification, the timestep was set to 1 fs.

Next, annealing simulations were performed, where the temperature of the simulation box was ramped up to 500 K. The temperature hold step was performed at 500 K in a controlled pressure and temperature (NPT) ensemble for 100 ps to ensure a stable elevated temperature throughout the simulation box. Furthermore, the simulation box was cooled to 300 K at a cooling rate of 50 K ns^{-1} in the NPT ensemble with "iso" settings, where the simulation box dimensions are controlled isometrically. Furthermore, another temperature hold step was performed at 300 K in the NPT ensemble with "aniso" settings to allow the simulation box to relax independently in all three directions. Annealing was performed to eliminate any unfavorable configurations of the monomers or GQD. For temperature hold and annealing, the timestep was set to 1 fs. Fig. 4(c) shows a snapshot of the MD model after densification and annealing simulations.

The crosslinking simulations followed the annealing step. The crosslinking simulations were performed to simulate the crosslinking of epoxy and to create the interfacial crosslinks between GQD and epoxy. Crosslinking was simulated by implementing the REACTER[59,60] algorithm in LAMMPS. The required reaction input files such as pre-reaction template, post-reaction template, and reaction map files were created to provide the reaction site topology and imported into LAMMPS. More details on the reaction template and map files can be found elsewhere.[59,61] Details about the epoxy crosslinking reaction and its mechanism are discussed in section S1 of the SI. Fig. S1 illustrates the 2-step crosslinking reaction simulated in this study. The temperature of the simulation box was increased from 300 K to 500 K in an NVT ensemble for increased mobility of the molecules. The crosslinking simulations were performed in an NVT ensemble at an elevated temperature of 500 K for 2 ns. The timestep was set to 1 fs. The reaction cutoff radius for epoxy crosslinking reactions was set to 6 Å, and the reaction probability was set to 0.0001. The

cutoff radius of 6 Å ensured the maximum crosslinking of the epoxy system with a realistic mass density comparable to the experimental value.

Fig. 4(d) shows the visualization of clusters in the epoxy-e4N-GQD nanocomposite model before and after crosslinking. Cluster analysis illustrates the number of clusters in the MD model by a unique color. Fig. 4(d) indicates the formation of a large epoxy network and the functionalization of the e4N-GQD and epoxy after crosslinking. The degree of crosslinking was calculated using

$$\text{Crosslinking density (\%)} = \frac{\text{total number of new bonds formed}}{\text{maximum number of bonds that can form}} \times 100 \quad (1)$$

For the functionalization of various GQDs, the respective reactions were modeled and simulated simultaneously with epoxy crosslinking. For amine-functionalized GQDs, crosslinks between functionalized amine groups and the epoxide groups on epoxy molecules were created. GQDs functionalized with epoxide groups were reacted with the amine groups in the hardener molecules, and carboxyl functional groups on GQDs were reacted with the epoxide groups on the epoxy molecules.[31] The GQDs with hydroxyl functional groups attached either on the surface or edge were not covalently bonded to epoxy due to unfavorable chemistry. The reaction cutoff radius for interfacial reactions was set to 6 Å, and the reaction probability was set to 0.1. The threshold radius and set probability ensure system stability and maximize the extent of the reaction.

Following the crosslinking simulations, another annealing step was performed for polymer network equilibration. For post-crosslinking annealing, the temperature of the simulation box was decreased from 500 K to 300 K at a cooling rate of 50 K ns^{-1} in the NPT ensemble with "iso" settings. This step was followed by a relaxation simulation at 300 K in the NPT ensemble with "aniso" settings for a 1 ns simulation time. For each epoxy nanocomposite model, 5 replicate models were created to account for statistical variation in MD predicted properties. Thus, including neat epoxy, a total of 50 unique MD models were created.

2.3. Mechanical testing simulations

To predict the mechanical properties, the simulation box was deformed unidirectionally in the *x*-, *y*-, and *z*-directions, respectively. The total strain applied was 20% at a constant strain rate of 2×10^8 s^{-1} in an NPT ensemble at 300 K. The timestep was set to 0.5 fs. The stress tensor was computed using the "compute pressure" command in LAMMPS. In LAMMPS, the stress tensor was computed using:

$$P_{ij} = \frac{1}{V}\sum_{k=1}^{N} m_k v_{k_i} v_{k_j} + \frac{1}{V}\sum_{k=1}^{N'} r_{k_i} f_{k_j} \quad (2)$$

where i and j are x, y, or z, V is the volume, N is the number of atoms, m is the mass of the atom, v is the velocity of the atom, N' is the total number of atoms including ghost atoms in neighboring subdomains due to periodicity, r is the position of the atom, and f is the force on the atom. The average unidirectional stresses were computed every 2000 timesteps. True strains were computed using the simulation box dimensions every timestep. A total of 150 MD simulations were performed for 50 unique MD models of neat epoxy and epoxy nanocomposites. Fig. 4(e) shows the MD setup of the mechanical testing simulations for a representative e4N-GQD-epoxy nanocomposite model.

Stress–strain plots were analyzed using LUNAR to calculate the Young's modulus and yield strength, as shown in Fig. 4(f).[62] LUNAR utilizes the Regression Fringe Response (RFR) method developed by Kemppainen *et al.*[62] In the RFR method, the linear region, non-linear region, and plastic regions are identified in the stress–strain plot. The RFR method employs calculations of the fringe slope to measure the change in linearity of the data to identify these regions. Furthermore, the slope of the linear region is used to calculate the Young's modulus. The yield point is identified by determining the first minima in the second derivative of the fringe slope of the stress–strain data. Further details about this method can be found elsewhere.[62] More details on the calculation of mechanical properties are provided in section S2 of the SI. Fig. S2 shows the plot of stress as a function of true strain for a representative e6N-GQD-Epoxy nanocomposite model in the *x*-direction. Fig. S3 in the SI shows the RFR analysis charts of the same system to determine the linear region and yield point. Poisson's ratio was predicted by analyzing the transverse strain *versus* axial strain plots using LUNAR. The average of the two transverse directions was reported as a final Poisson's ratio for a given MD model. Fig. S4 shows a representative transverse strain analysis for the representative epoxy nanocomposite. The predicted mechanical properties were calculated by averaging the values for all three directions over five replicate models.

Furthermore, the free volume analysis of the MD models before and after the mechanical testing was performed using LUNAR. For the free volume analysis, the probe of 1.1 Å was used and the voxel size of 0.5 Å. More details on the methodology of free volume analysis in LUNAR can be found elsewhere.[50]

3. Results and discussion

Table 2 shows the comparison of the density predicted in this work using IFF with previously predicted density values with IFF and ReaxFF forcefield by Deshpande *et al.*[31] and Keles *et al.*[32] The predicted density values of neat epoxy are in agreement with the previously reported IFF values. Furthermore, the predicted density values of functionalized GQD models are consistent with the neat epoxy density. The predicted density value of neat epoxy matches the experimentally measured density value of 1.193 ± 0.001 by Odegard *et al.*[17]

Fig. 5 shows the plot of MD-predicted Young's moduli of various epoxy material systems. The MD predicted Young's

Table 2 MD predicted density of epoxy nanocomposites

Material	Crosslinking density (%)	IFF (g cm^{-3})	ReaxFF (g cm^{-3})
Neat epoxy	82 ± 4	1.189 ± 0.007	1.226 ± 0.003[a]
GQD-Epoxy	91 ± 3	1.194 ± 0.007	1.226 ± 0.001[a]
e4N-GQD-Epoxy	85 ± 4	1.191 ± 0.007	1.230 ± 0.001[b]
e6N-GQD-Epoxy	84 ± 4	1.192 ± 0.012	1.240 ± 0.001[b]
e4COOH-GQD-Epoxy	85 ± 1	1.192 ± 0.012	1.233 ± 0.003[a]
s4O-GQD-Epoxy	92 ± 2	1.198 ± 0.005	1.235 ± 0.002[a]
s4OH-GQD-Epoxy	90 ± 1	1.193 ± 0.008	1.233 ± 0.003[a]
s8OH-GQD-Epoxy	85 ± 1	1.195 ± 0.005	1.233 ± 0.003[a]
e4OH-s4OH-Epoxy	90 ± 1	1.203 ± 0.007	1.232 ± 0.004[a]
e4COOH-s4OH-Epoxy	85 ± 1	1.194 ± 0.004	1.229 ± 0.002[a]

[a] MD predictions by Deshpande *et al.*[31] [b] MD predictions by Keles *et al.*[32]

modulus of neat epoxy is in agreement with the experimentally measured value by Littell *et al.*[15] and Gilat *et al.*[18] and the MD-predicted value using ReaxFF by Deshpande *et al.*[31] Young's modulus of the amine-functionalized GQD–epoxy nanocomposite is predicted to be the highest among the set modeled herein. Amine-functionalized GQDs show improved Young's modulus compared to the GQD–epoxy nanocomposite due to covalent functionalization between GQDs and epoxy. The predicted modulus for e4N-GQD and e6N-GQD epoxy models is 3.5 ± 0.2 GPa, compared to 3.1 ± 0.1 GPa of neat epoxy, demonstrating a 13% increase. However, there is no significant improvement in the Young's modulus of epoxy with eCOOH-GQD, surface epoxide, and surface hydroxyl functionalized GQDs. The e4COOH-s4O-GQD shows improvement in the Young's modulus predicted by IFF compared to neat epoxy and is comparable to amine-functionalized GQD nanocomposites.

Fig. 5 also shows that the Young's modulus predicted by IFF is higher than the ReaxFF predictions for pristine GQD, e4N-GQD, e6N-GQD, and e4COOH-s4O-GQD epoxy nanocomposites; while it is lower for s8OH-GQD and e4OH-s4O-GQD epoxy. Whereas for e4COOH-GQD, s4O-GQD, and s4OH-GQD epoxy, the predictions by IFF and ReaxFF match very well. The discrepancies observed in the predictions of Young's modulus are due to the inherent nature of defined bonds in IFF *vs.* bond-order-based bonds in ReaxFF. Since IFF includes fixed bonds, the covalent bonds in the bonded GQDs, such as amine-functionalized GQDs, add to the rigidity in the backbone of the network during deformation and hence the overprediction compared to ReaxFF models, whereas this effect is not observed in the hydroxyl functionalized nanocomposites that are not covalently bonded to the epoxy.

Fig. 6 shows the plot of yield strengths of epoxy–GQD nanocomposites predicted by MD simulations using IFF, and they are compared with ReaxFF predictions by Deshpande *et al.*[31] The IFF predicted yield strength of neat epoxy models agrees very well with the experimentally measured strength values by Littell *et al.*[15] and Gilat *et al.*,[18] as shown in Fig. 6. The ReaxFF predictions of the yield strength of neat epoxy show significant overprediction. The overprediction of the yield strength of neat epoxy has already been reported previously by different MD studies.[63,64] The trend in the yield strength predicted by IFF matches the previous ReaxFF predictions except for the e4COOH-GQD-epoxy system.

The overprediction of the ReaxFF yield strength values is consistent through various epoxy nanocomposites in comparison with the IFF predicted yield strength values. These overpredictions are attributed to the predefined bond flexibility in IFF *vs.* the bond-order-based connectivity in ReaxFF. IFF includes fixed bonds that predefine the connectivity in addition to other bonded interactions such as angles, dihedrals, impro-

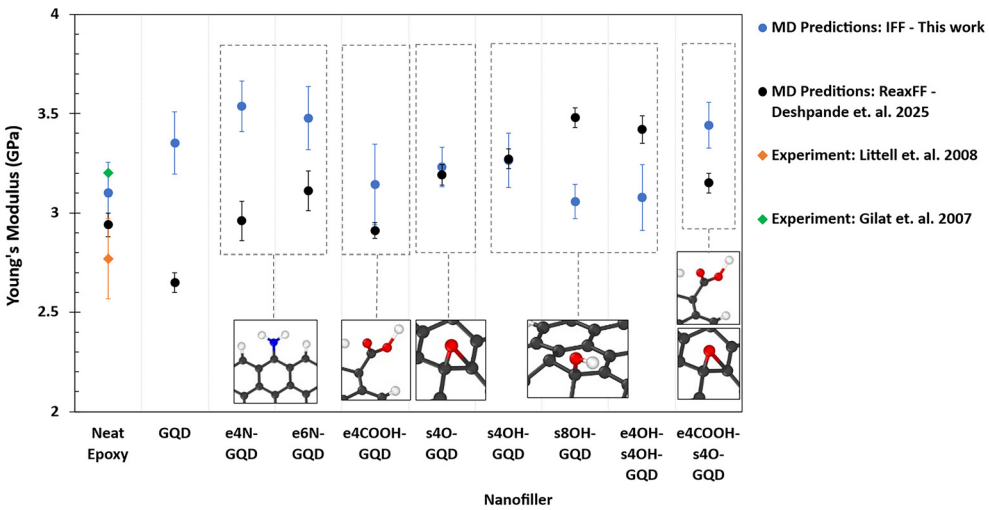

Fig. 5 MD-predicted Young's moduli of epoxy nanocomposites with various GQD nanofillers. Snapshots of the MD models show the functional groups attached to GQDs in the respective nanocomposite. Atom colors are assigned as carbon in black, oxygen in red, hydrogen in white, and nitrogen in blue.

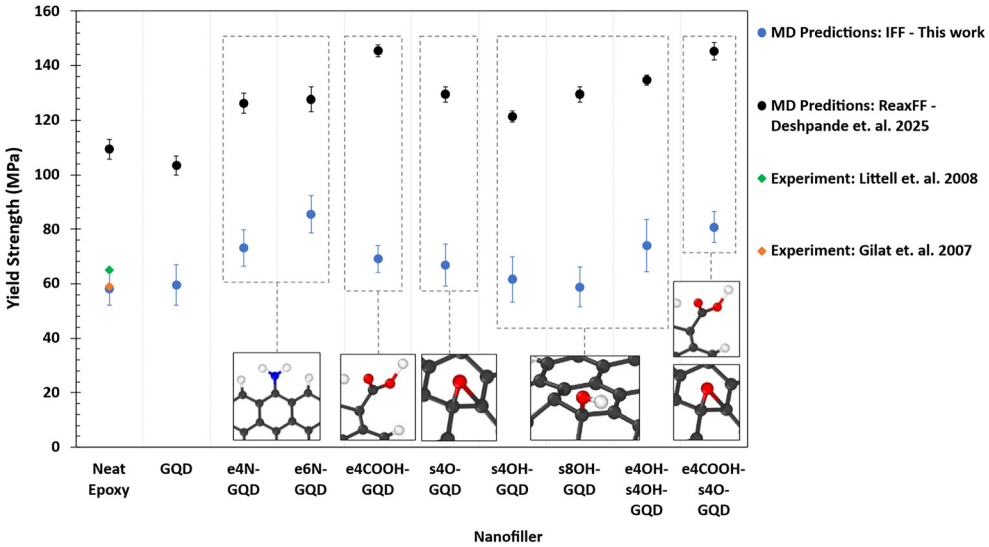

Fig. 6 Plot of MD-predicted yield strengths of epoxy nanocomposites with various GQD nanofillers. Snapshots of the MD models show the functional groups attached to GQDs in the respective nanocomposite. Atom colors are assigned as carbon in black, oxygen in red, hydrogen in white, and nitrogen in blue.

pers, and cross-terms that allow flexibility of molecules under the applied load, whereas bond orders utilized in ReaxFF lead to overpredictions due to the unavailability of different atom types based on functional groups and higher energy terms.[36]

Overall, functionalized GQDs improve the yield strength of epoxy, as shown in Fig. 6. The e6N-GQD-epoxy nanocomposite exhibits the highest yield strength of 85 ± 9 MPa among the material systems modeled in this study, representing a 47% increase compared to neat epoxy. Fig. 6 shows that there is no statistical difference in the improvement in the yield strength of epoxy with e4COOH-GQD, surface epoxide, and surface hydroxyl functionalized GQDs. e4COOH-s4O-GQD-epoxy is predicted to have a yield strength of 81 ± 4 MPa, demonstrating a 40% increase in the yield strength.

The pristine GQD–epoxy nanocomposite exhibits an 8% increase in the Young's modulus as shown in Fig. 5, whereas Fig. 6 shows that there is no improvement in the yield strength compared to neat epoxy. This indicates that the pristine GQD improves the stiffness of the epoxy. It is clear that the addition of covalent functionalization between epoxy and GQD further improves the modulus and strength, showing improved load transfer between the polymer and nanofiller.

Fig. 7 shows the plot of potential energy distribution amongst bonded and non-bonded energy terms. Fig. 7 illustrates the contribution of the energy term towards the total potential energy of the respective material system. The contribution of the % bond energy remains consistent in all the materials, irrespective of GQD insertion. The pairwise and improper energy contributions show minimal effect on the total potential energy in all material systems. The % dihedral energy increases with the inclusion of GQD as seen in Fig. 7. The contribution of dihedral energy in the neat epoxy material is 11.6 ± 0.1%, which increases to 24.4 ± 0.5% in the pristine GQD–epoxy nanocomposite material. The highest increases in the dihedral energy contribution are observed in the e6N-GQD-epoxy nanocomposite material as 26.5 ± 0.4%.

Dihedral energy is the potential energy associated with the rotation of the polymer chain around a covalent bond. Higher dihedral energy corresponds to a rigid dihedral potential function, which can be translated to a stiffer response in real-world applications. This means, higher energy is required to twist the bond; therefore, the material exhibits increased resistance to deformation. Polymers or 2D materials such as graphene, with stiff dihedral terms, display restricted movement along the chain and exhibit reduced flexibility.[65] When external strain or deformation is applied, these stiff dihedrals are unable to reconfigure to absorb additional energy caused due to deformation. Hence, the material exhibits higher stiffness and modulus. This can be observed in Fig. 5 and 6, where amine-functionalized epoxy is predicted to show improved modulus and strength among the materials systems studied here.

Fig. 8 shows the change in the energy terms during the tensile simulation of a representative e6N-GQD-epoxy nanocomposite in the *x*-direction. Fig. 8 shows that the linear region was identified using the LUNAR tool in the raw MD data using the RFR method. The predicted yield strength is 66.4 MPa and the Young's modulus is 3.96 GPa. Overall, the potential energy, dihedral energy, and van der Waals' energy of the material increase with an increase in the strain. However, bond energy, angle energy, and improper energy of the material are insensitive to the applied strain.

The region R1 is in the linear region of the stress–strain plot. The potential energy of the material in the linear region is constant and does not change with deformation as shown in Fig. 8. However, the potential energy increases as soon as the

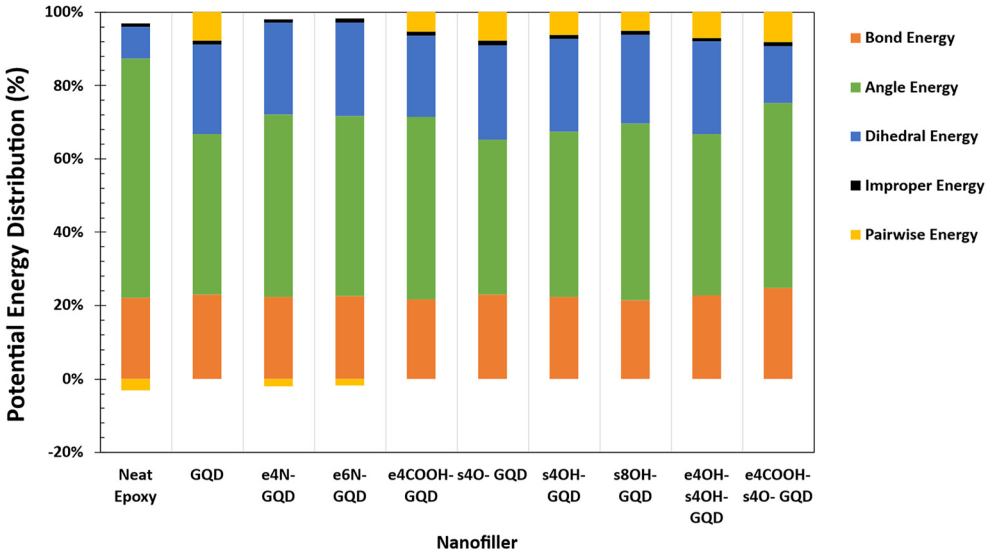

Fig. 7 Plot of potential energy distribution into bonded and non-bonded energy terms. Non-bonded energy terms are shown as pairwise energy; bonded energy is further segregated into bond, angle, dihedral, and improper energy.

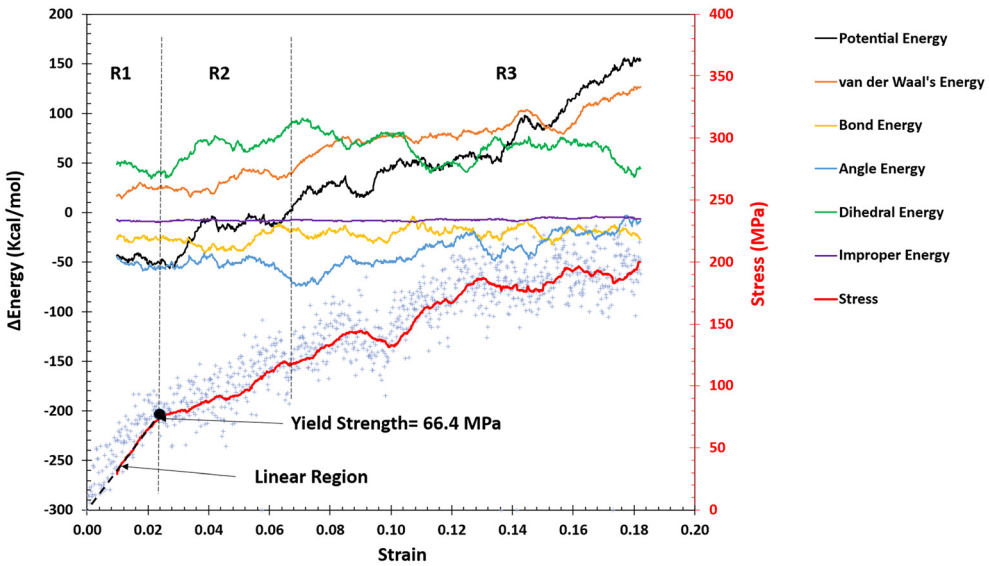

Fig. 8 Plot of bonded and non-bonded energies as a function of strain of a representative tensile MD simulation of the e6N-GQD-epoxy nanocomposite in the *x*-direction. Change in the energy is plotted on the primary *y*-axis, and stress is plotted on the secondary *y*-axis. The solid lines represent the moving average of the MD simulation data. Purple colored datapoints show the raw MD simulation stress data. The raw MD data of energies are not shown for clarity of the plot. Dotted vertical lines are to represent the three regions such as R1, R2, and R3 in the plot.

yield point is reached at 2.1% strain. This increase can clearly be seen in the R2 region of Fig. 8. This increase in the potential energy is largely due to the increase in the dihedral energy in the material. With further increases in strain to 7%, the material's stiffer response due to dihedrals drops down as the change in the dihedral energy is constant thereafter. The R3 region shows that the increases in the potential energy are observed solely due to increases in the van der Waals' energy terms. It is important to note that the change in the van der Waals' energy is reported and is positive, showing that the net van der Waals' energy is going closer to zero with deformation.

Fig. 9(a) shows the predictions of Poisson's ratio of neat epoxy and various epoxy nanocomposites. The Poisson's ratio values predicted by IFF show no statistical effect of the inclusion of GQDs in the epoxy. The Poisson's ratio predicted by both IFF and ReaxFF of neat epoxy matches the experimentally calculated values.[15,18] Higher discrepancies are observed in the predictions of Poisson's ratio predicted by IFF and ReaxFF for nanocomposite models with various GQDs.

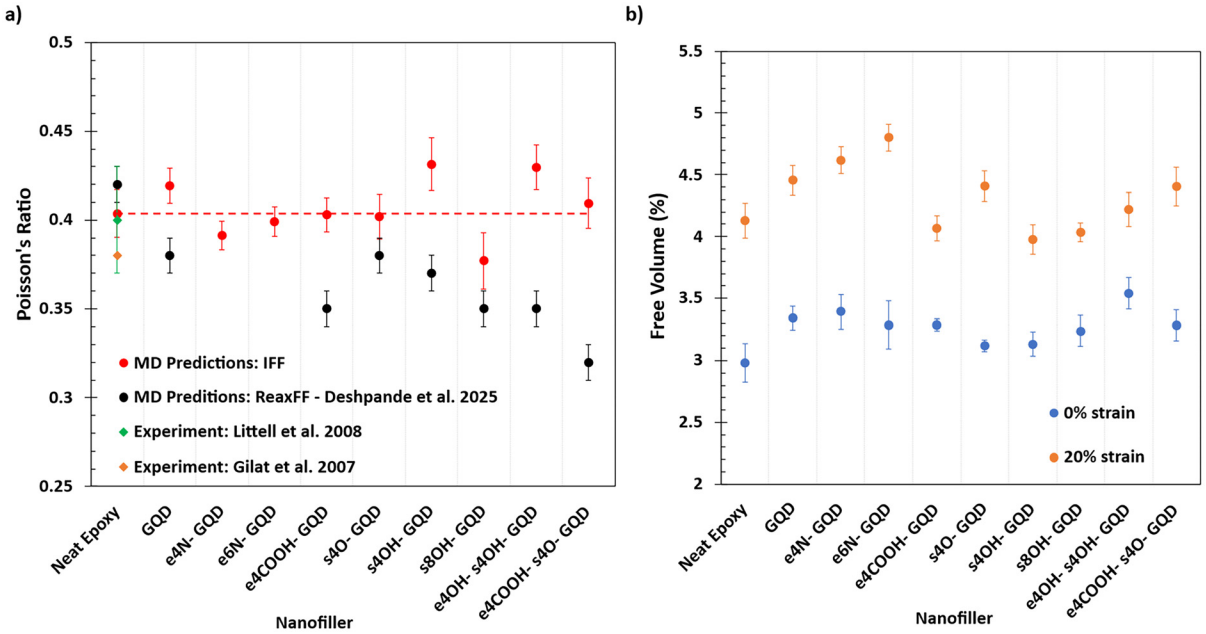

Fig. 9 Plot of (a) MD-predicted Poisson's ratio of epoxy nanocomposites. Neat epoxy predictions are compared with experimental measurements from the literature.[15,18] (b) % Free volume in the epoxy nanocomposite MD models at 0% and 20% strain.

Fig. 9(b) shows the % free volume in the epoxy nanocomposite MD models at 0% strain and 20% strain. Compared to neat epoxy, all epoxy nanocomposites exhibit an increase in the free volume. Inclusion of any GQD increases the free volume in the epoxy due to its rigid planar structure. For small local regions around the GQD, polymer chains are constrained, causing polymer network configurations to reorganize leading to an increase in free volume and non-uniform density in the model as shown in Fig. S3 in the SI.

All of the epoxy nanocomposites exhibit an increase in the % free volume after the deformation as expected. Hydroxyl and carboxyl functionalized GQDs show a comparatively lower increase in the free volume compared to amine functionalized GQDs after deformation. Oxygen atoms in the hydroxyl and

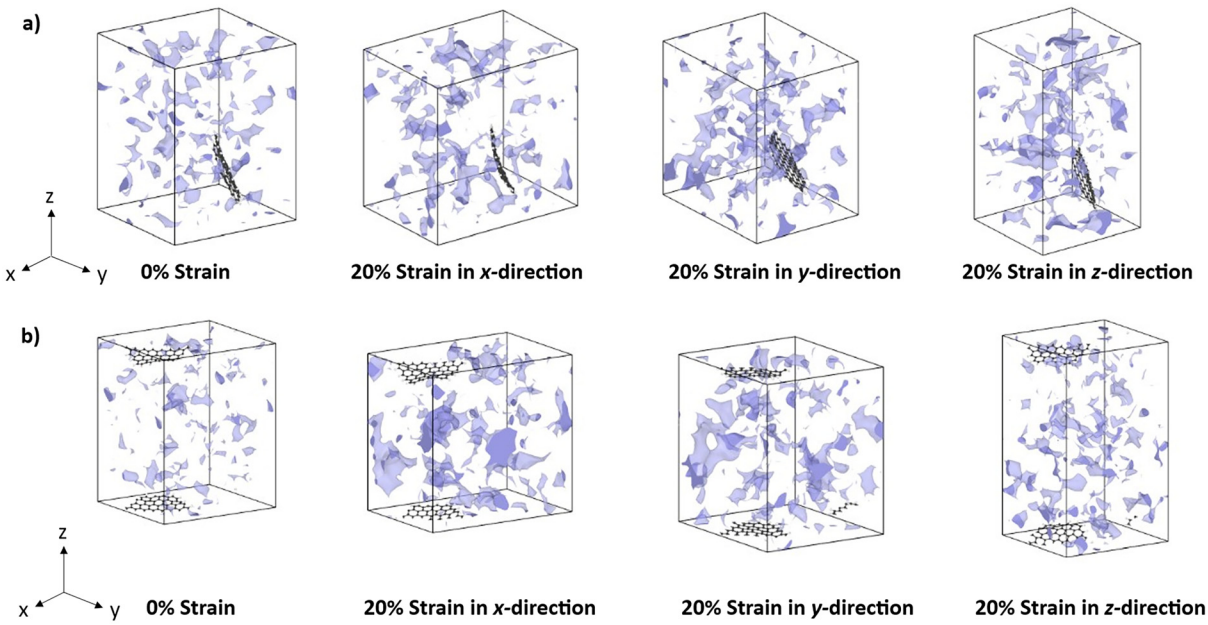

Fig. 10 Visualization of free volume at 0% strain, 20% strain in the *x*-direction, 20% strain in the *y*-direction, and 20% strain in the *z*-direction for (a) GQD-epoxy and (b) e6N-GQD-epoxy nanocomposites.

carboxyl functional groups are more electronegative compared to nitrogen atoms in amine groups; therefore, stronger hydrogen bonding interactions are predicted, which results in lower increases in free volume after deformation. The increase of free volume is predicted to be the lowest in neat epoxy and hydroxyl functionalized GQD nanocomposites. The e6N-GQD-epoxy nanocomposite exhibits the highest increase in the free volume after deformation as seen in Fig. 9(b).

Fig. 10 illustrates the increase of free volume pockets in a representative GQD-epoxy and e6N-GQD-epoxy model after deformation in the *x*, *y*, and *z*-directions. Fig. 10(a) shows that the pristine GQD-epoxy models show free volume spread across the materials system with a significant presence of free volume pockets around the GQD. Since the pristine GQD is neither covalently bonded with the epoxy nor is functionalized with surface epoxide or hydroxyl groups, the GQD molecules are less restricted compared to functional GQDs. This creates free volume pockets around the GQD as seen in Fig. 10(a). As the MD model is deformed in the *x*, *y*, and *z*-directions, Fig. 10(a) shows that the increase of free volume is observed in both the epoxy network and the free volume around the GQD. Specifically, the free volume increase is more prominent around the GQD in the case of transverse loading to the plane of the GQD; in this case, it is observed in the *y*-direction deformation.

From Fig. 10(b), it can be clearly seen that the free volume pockets in the MD models increase in the direction of the applied strain. The e6N-GQD is shown to have minimal effects on the increase of the free volume in the MD models. The increase of free volume is primarily observed in the epoxy network. This provides more qualitative insights into stronger interfacial and functional interactions between e6N-GQD and the epoxy network. In the case of transverse loading with respect to the GQD plane, *i.e.*, *z*-direction, the e6N-GQD does not exhibit free volume increase around the GQD, indicating improved interfacial interactions with epoxy.

4. Conclusion

This research effort provides information about the influence of various functional GQDs on the mechanical properties of the epoxy. The MD predicted materials properties in this study are consistent with experimentally measured values for neat epoxy. Below are the important conclusions that can be drawn from this study.

1. MD predictions of Young's modulus and yield strength are accurate using IFF compared to ReaxFF predictions.

2. The amine-functionalized GQD shows the highest 14% improvement in the Young's modulus. Edge functionalization of amine groups exhibits an improved Young's modulus compared to surface functionalization of hydroxyl and epoxide functional groups. GQDs functionalized with carboxyl groups on edges and epoxide on the surface show a significant improvement of 11% in the Young's modulus.

3. The amine-functionalized GQD shows the highest 47% increase in the yield strength. GQDs with carboxyl and epoxide functional groups show a significant improvement of 39% in the yield strength.

4. There is no statistical difference in the predicted Poisson's ratio of the various GQD–epoxy nanocomposites.

5. Functionalization of GQDs affects the free volume increase in the epoxy nanocomposites during deformation. Functionalization improves the interfacial interactions between GQD and epoxy, thereby improving mechanical behavior at the nanoscale.

These conclusions support that the mechanical properties of the epoxy can be tailored significantly for improved performance of PMCs using GQDs. The findings of this study suggest the use of the IFF forcefield for accurate and efficient predictions of materials properties of the polymer nanocomposites, thereby accelerating the materials discovery through physics-informed artificial intelligence. This study provides a significant understanding of the role of functionalization of GQDs in the design and development of next generation high-performance composites for structural applications in aerospace and defense.

Conflicts of interest

There are no conflicts of interest to declare.

Data availability

Data for this article, including MD modeling scripts, MD structures, MD simulation files for mechanical testing, analysis files for mechanical properties, and analysis files for free volume analysis, are available at Mendeley Data at Swapnil Sambhaji Bamane and Ozgur Keles (2025), "Molecular Dynamics Simulation Data for Prediction of Mechanical Properties of Epoxy with Graphene Quantum Dots", Mendeley Data, V2, at https://doi.org/10.17632/n8fnmb89jr.2.

Additionally, the MD structures developed in ReaxFF are available at https://doi.org/10.17632/nvrkj7cygx.2.

Supplementary information (SI): stress–strain plot analysis, Poisson's ratio calculation, and density distribution analysis. See DOI: https://doi.org/10.1039/d5lp00373c.

Acknowledgements

This research was supported by a U.S. National Science Foundation CAREER award, grant #2450841. STARLIGHT, a high-performance computing cluster at the University of North Carolina at Charlotte, was used to perform MD simulations presented in this publication.

References

1 M.-F. Yu, O. Lourie, M. J. Dyer, K. Moloni, T. F. Kelly and R. S. Ruoff, Strength and Breaking Mechanism of

Multiwalled Carbon Nanotubes Under Tensile Load, *Science*, 2000, **287**(5453), 637–640.
2 R. D. Downes, A. Hao, J. G. Park, Y.-F. Su, R. Liang, B. D. Jensen, E. J. Siochi and K. E. Wise, Geometrically constrained self-assembly and crystal packing of flattened and aligned carbon nanotubes, *Carbon*, 2015, **93**, 953–966.
3 A. Mahmud, H. Radue, M. S. Pisani, W. A. Odegard and G. M, Computational Modeling of Hybrid Carbon Fiber/Epoxy Composites Reinforced with Functionalized and Non-Functionalized Graphene Nanoplatelets, *Nanomaterials*, 2021, **11**(11), 2919.
4 C. M. Hadden, D. R. Klimek-McDonald, E. J. Pineda, J. A. King, A. M. Reichanadter, I. Miskioglu, S. Gowtham and G. M. Odegard, Mechanical properties of graphene nanoplatelet/carbon fiber/epoxy hybrid composites: Multiscale modeling and experiments, *Carbon*, 2015, **95**, 100–112.
5 I. A. Kinloch, J. Suhr, J. Lou, R. J. Young and P. M. Ajayan, Composites with carbon nanotubes and graphene: An outlook, *Science*, 2018, **362**(6414), 547–553.
6 A. Mahmud, H. Radue, M. S. Chinkanjanarot, S. Odegard and G. M, Multiscale Modeling of Epoxy-Based Nanocomposites Reinforced with Functionalized and Non-Functionalized Graphene Nanoplatelets, *Polymers*, 2021, **13**(12), 1958.
7 P. Deshpande, S. Shah, S. Patil, M. Olaya, G. Odegard and M. Maiaru, Process modelling the cure of bisphenol-A Epoxy/Jeffamine system using ICME, in Proceedings of the American Society for Composites- Thirty-Sixth Technical Conference on Composite Materials, 2021.
8 A. Gao, Y. Gu, Q. Wu, C. Yuan, M. Li and Z. Zhang, Influence of processing temperature on interfacial behavior of HKT800 carbon fiber with BMI and epoxy matrices, *Chin. J. Aeronaut.*, 2015, **28**(4), 1255–1262.
9 R. Hsissou, R. Seghiri, Z. Benzekri, M. Hilali, M. Rafik and A. Elharfi, Polymer composite materials: A comprehensive review, *Compos. Struct.*, 2021, **262**, 113640.
10 D. J. O'Brien and S. R. White, Cure kinetics, gelation, and glass transition of a bisphenol F epoxide, *Polym. Eng. Sci.*, 2003, **43**(4), 863–874.
11 G. M. Odegard and A. Bandyopadhyay, Physical aging of epoxy polymers and their composites, *J. Polym. Sci., Part B: Polym. Phys.*, 2011, **49**(24), 1695–1716.
12 S. U. Patil, J. Kemppainen, M. Maiaru and G. M. Odegard, High-performance, multi-component epoxy resin simulation for predicting thermo-mechanical property evolution during curing, *Polym. J.*, 2025, 539–552.
13 L. Yao, M. Li, Q. Wu, Z. Dai, Y. Gu, Y. Li and Z. Zhang, Comparison of sizing effect of T700 grade carbon fiber on interfacial properties of fiber/BMI and fiber/epoxy, *Appl. Surf. Sci.*, 2012, **263**, 326–333.
14 A. Kausar, I. Rafique and B. Muhammad, Review of Applications of Polymer/Carbon Nanotubes and Epoxy/CNT Composites, *Polym.-Plast. Technol. Eng.*, 2016, **55**(11), 1167–1191.
15 J. D. Littell, C. R. Ruggeri, R. K. Goldberg, G. D. Roberts, W. A. Arnold and W. K. Binienda, Measurement of Epoxy Resin Tension, Compression, and Shear Stress–Strain Curves over a Wide Range of Strain Rates Using Small Test Specimens, *J. Aerosp. Eng.*, 2008, **21**(3), 162–173.
16 S. J. Tucker, *Study of 3, 3′ vs. 4, 4′ DDS isomer curatives on physical properties and phenyl ring motions of DGEBA epoxy via molecular dynamics, deuterium NMR, and dielectric spectroscopy*, The University of Southern Mississippi, 2010.
17 G. M. Odegard, S. U. Patil, P. P. Deshpande, K. Kanhaiya, J. J. Winetrout, H. Heinz, S. P. Shah and M. Maiaru, Molecular Dynamics Modeling of Epoxy Resins Using the Reactive Interface Force Field, *Macromolecules*, 2021, **54**(21), 9815–9824.
18 A. Gilat, R. K. Goldberg and G. D. Roberts, Strain Rate Sensitivity of Epoxy Resin in Tensile and Shear Loading, *J. Aerosp. Eng.*, 2007, **20**(2), 75–89.
19 S. Chatterjee, J. W. Wang, W. S. Kuo, N. H. Tai, C. Salzmann, W. L. Li, R. Hollertz, F. A. Nüesch and B. T. T. Chu, Mechanical reinforcement and thermal conductivity in expanded graphene nanoplatelets reinforced epoxy composites, *Chem. Phys. Lett.*, 2012, **531**, 6–10.
20 D. R. Bortz, E. G. Heras and I. Martin-Gullon, Impressive Fatigue Life and Fracture Toughness Improvements in Graphene Oxide/Epoxy Composites, *Macromolecules*, 2012, **45**(1), 238–245.
21 B. Ahmadi-Moghadam, M. Sharafimasooleh, S. Shadlou and F. Taheri, Effect of functionalization of graphene nanoplatelets on the mechanical response of graphene/epoxy composites, *Mater. Des.*, 1980, **66**, 142–149.
22 S. Liu, V. S. Chevali, Z. Xu, D. Hui and H. Wang, A review of extending performance of epoxy resins using carbon nanomaterials, *Composites, Part B*, 2018, **136**, 197–214.
23 S. R. Mousavi, S. Estaji, A. Paydayesh, M. Arjmand, S. H. Jafari, S. Nouranian and H. A. Khonakdar, A review of recent progress in improving the fracture toughness of epoxy-based composites using carbonaceous nanofillers, *Polym. Compos.*, 2022, **43**(4), 1871–1886.
24 M. Rallini and J. M. Kenny, 3 - Nanofillers in Polymers, in *Modification of Polymer Properties*, ed. C. F. Jasso-Gastinel and J. M. Kenny, William Andrew Publishing, 2017, pp. 47–86.
25 R. C. Voicu, M. Gologanu, C. Tibeica, M. Santiago-Calvo, M. Asensio, E. Cañibano, O. Nedelcu and T. Sandu, Prediction of Mechanical Properties of Nano-Clay-Based Biopolymeric Composites, *Nanomaterials*, 2024, **14**(17), 1403.
26 L.-C. Tang, X. Wang, Y.-J. Wan, L.-B. Wu, J.-X. Jiang and G.-Q. Lai, Mechanical properties and fracture behaviors of epoxy composites with multi-scale rubber particles, *Mater. Chem. Phys.*, 2013, **141**(1), 333–342.
27 N. Payungwong, J. Wu and J. Sakdapipanich, Unlocking the potential of natural rubber: A review of rubber particle sizes and their impact on properties, *Polymer*, 2024, **308**, 127419.

28 N. Domun, H. Hadavinia, T. Zhang, T. Sainsbury, G. H. Liaghat and S. Vahid, Improving the fracture toughness and the strength of epoxy using nanomaterials – a review of the current status, *Nanoscale*, 2015, **7**(23), 10294–10329.

29 P. K. Balguri, D. G. H. Samuel and U. Thumu, A review on mechanical properties of epoxy nanocomposites, *Mater. Today: Proc.*, 2021, **44**, 346–355.

30 A. Nag, R. B. V. B. Simorangkir, D. R. Gawade, S. Nuthalapati, J. L. Buckley, B. O'Flynn, M. E. Altinsoy and S. C. Mukhopadhyay, Graphene-based wearable temperature sensors: A review, *Mater. Des.*, 2022, **221**, 110971.

31 P. P. Deshpande, R. Chan-Jobe, J. Kemppainen, G. M. Odegard and O. Keles, Optimizing Epoxy Nanocomposites with Oxidized Graphene Quantum Dots for Superior Mechanical Performance: A Molecular Dynamics Approach, *ACS Omega*, 2025, **10**(14), 14209–14220.

32 Ö. Keleş and P. P. Deshpande, Mechanical behavior of graphene quantum dot epoxy nanocomposites: A molecular dynamics study, *Mater. Lett.*, 2024, **362**, 136206.

33 J. R. Seibert, Ö. Keleş, J. Wang and F. Erogbogbo, Infusion of graphene quantum dots to modulate thermal conductivity and dynamic mechanical properties of polymers, *Polymer*, 2019, **185**, 121988.

34 A. Bokare, D. Nordlund, C. Melendrez, R. Robinson, O. Keles, A. Wolcott and F. Erogbogbo, Surface functionality and formation mechanisms of carbon and graphene quantum dots, *Diamond Relat. Mater.*, 2020, **110**, 108101.

35 L. Pauling, The nature of the chemical bond—1992, *J. Chem. Educ.*, 1992, **69**(7), 519.

36 J. J. Winetrout, K. Kanhaiya, J. Kemppainen, P. J. Veld, G. Sachdeva, R. Pandey, B. Damirchi, A. van Duin, G. M. Odegard and H. Heinz, Implementing reactivity in molecular dynamics simulations with harmonic force fields, *Nat. Commun.*, 2024, **15**(1), 7945.

37 S. S. Bamane, P. P. Deshpande, S. U. Patil, M. Maiaru and G. M. Odegard, Evolution of Physical, Thermal, and Mechanical Properties of Poly(methyl Methacrylate)-Based Elium Thermoplastic Polymer During Polymerization, *J. Phys. Chem. C*, 2024, **128**(37), 15639–15648.

38 S. S. Bamane, P. S. Gaikwad, M. S. Radue, S. Gowtham and G. M. Odegard, Wetting Simulations of High-Performance Polymer Resins on Carbon Surfaces as a Function of Temperature Using Molecular Dynamics, *Polymers*, 2021, **13**(13), 2162.

39 S. S. Bamane, M. B. Jakubinek, K. Kanhaiya, B. Ashrafi, H. Heinz and G. M. Odegard, Boron Nitride Nanotubes: Force Field Parameterization, Epoxy Interactions, and Comparison with Carbon Nanotubes for High-Performance Composite Materials, *ACS Appl. Nano Mater.*, 2023, **6**(5), 3513–3524.

40 G. Sachdeva, S. U. Patil, S. S. Bamane, P. P. Deshpande, W. A. Pisani, G. M. Odegard and R. Pandey, Mechanical response of polymer/BN composites investigated by molecular dynamics method, *J. Mater. Res.*, 2022, **37**(24), 4533–4543.

41 P. Gaikwad, A. Krieg, P. Deshpande, S. Patil, J. King, M. Maiaru and G. Odegard, Understanding the Origin of the Low Cure Shrinkage of Polybenzoxazine Resin by Computational Simulation, *ACS Appl. Polym. Mater.*, 2021, **3**(12), 6407–6415.

42 S. U. Patil, A. S. Krieg, L. K. Odegard, U. Yadav, J. A. King, M. Maiaru and G. M. Odegard, Simple and convenient mapping of molecular dynamics mechanical property predictions of bisphenol-F epoxy for strain rate, temperature, and degree of cure, *Soft Matter*, 2023, **19**(35), 6731–6742.

43 K. Kashmari, H. Al Mahmud, S. U. Patil, W. A. Pisani, P. Deshpande, M. Maiaru and G. M. Odegard, Multiscale Process Modeling of Semicrystalline PEEK for Tailored Thermomechanical Properties, *ACS Appl. Eng. Mater.*, 2023, **1**(11), 3167–3177.

44 P. P. Deshpande, M. S. Radue, P. Gaikwad, S. Bamane, S. U. Patil, W. A. Pisani and G. M. Odegard, Prediction of the Interfacial Properties of High-Performance Polymers and Flattened CNT-Reinforced Composites Using Molecular Dynamics, *Langmuir*, 2021, **37**(39), 11526–11534.

45 W. A. Pisani, M. S. Radue, S. U. Patil and G. M. Odegard, Interfacial modeling of flattened CNT composites with cyanate ester and PEEK polymers, *Composites, Part B*, 2021, **211**, 108672.

46 S. S. Bamane and O. Keles, Effects of Graphene Quantum Dots on Thermal Properties of Epoxy Using Molecular Dynamics, *Appl. Nano*, 2025, **6**(3), 15.

47 P. Deshpande, R. Chan-Jobe and O. Keles, Molecular structure data and modelling roadmap for optimized oxidized graphene quantum dot and epoxy interface and mechanical properties, *Data Brief*, 2024, **57**, 111059.

48 A. P. Thompson, H. M. Aktulga, R. Berger, D. S. Bolintineanu, W. M. Brown, P. S. Crozier, P. J. in't Veld, A. Kohlmeyer, S. G. Moore, T. D. Nguyen, R. Shan, M. J. Stevens, J. Tranchida, C. Trott and S. J. Plimpton, LAMMPS - a flexible simulation tool for particle-based materials modeling at the atomic, meso, and continuum scales, *Comput. Phys. Commun.*, 2022, **271**, 108171.

49 H. Heinz, T.-J. K. Lin, R. Mishra and F. S. Emami, Thermodynamically Consistent Force Fields for the Assembly of Inorganic, Organic, and Biological Nanostructures: The INTERFACE Force Field, *Langmuir*, 2013, **29**(6), 1754–1765.

50 J. Kemppainen, J. R. Gissinger, S. Gowtham and G. M. Odegard, LUNAR: Automated Input Generation and Analysis for Reactive LAMMPS Simulations, *J. Chem. Inf. Model.*, 2024, **64**(13), 5108–5126.

51 A. Stukowski, Visualization and analysis of atomistic simulation data with OVITO-the Open Visualization Tool, *Modell. Simul. Mater. Sci. Eng.*, 2010, **18**(1), 015012.

52 M. D. Hanwell, D. E. Curtis, D. C. Lonie, T. Vandermeersch, E. Zurek and G. R. Hutchison, Avogadro: an advanced semantic chemical editor, visualization, and analysis platform, *J. Cheminf.*, 2012, **4**(1), 17.

53 S. U. Patil, M. S. Radue, W. A. Pisani, P. Deshpande, H. Xu, H. Al Mahmud, T. Dumitrică and G. M. Odegard,

Interfacial characteristics between flattened CNT stacks and polyimides: A molecular dynamics study, *Comput. Mater. Sci.*, 2020, **185**, 109970.

54 N. Gobi, D. Vijayakumar, O. Keles and F. Erogbogbo, Infusion of Graphene Quantum Dots to Create Stronger, Tougher, and Brighter Polymer Composites, *ACS Omega*, 2017, **2**(8), 4356–4362.

55 D. A. Evans, History of the Harvard ChemDraw Project, *Angew. Chem., Int. Ed.*, 2014, **53**(42), 11140–11145.

56 J. Petrović, D. Bekric, I. Vujčić, I. Dimic and S. Putić, Microstructural characterization of glass-epoxy composites subjected to tensile testing, *Acta Period. Technol.*, 2013, **44**, 151–162.

57 C. M. Hadden, B. D. Jensen, A. Bandyopadhyay, G. M. Odegard, A. Koo and R. Liang, Molecular modeling of EPON-862/graphite composites: Interfacial characteristics for multiple crosslink densities, *Compos. Sci. Technol.*, 2013, **76**, 92–99.

58 G. M. Odegard, S. U. Patil, P. S. Gaikwad, P. Deshpande, A. S. Krieg, S. P. Shah, A. Reyes, T. Dickens, J. A. King and M. Maiaru, Accurate predictions of thermoset resin glass transition temperatures from all-atom molecular dynamics simulation, *Soft Matter*, 2022, **18**(39), 7550–7558.

59 J. R. Gissinger, B. D. Jensen and K. E. Wise, REACTER: A Heuristic Method for Reactive Molecular Dynamics, *Macromolecules*, 2020, **53**(22), 9953–9961.

60 J. R. Gissinger, B. D. Jensen and K. E. Wise, Modeling chemical reactions in classical molecular dynamics simulations, *Polymer*, 2017, **128**, 211–217.

61 J. R. Gissinger, B. D. Jensen and K. E. Wise, Molecular modeling of reactive systems with REACTER, *Comput. Phys. Commun.*, 2024, **304**, 109287.

62 J. Kemppainen, G. Odegard, T. Muzzy and T. Wavrunek, Understanding and Interpreting Stress–Strain Curves from Molecular Dynamics Simulation of Amorphous Polymers, in ChemRxiv, 2025.

63 M. S. Radue, B. D. Jensen, S. Gowtham, D. R. Klimek-McDonald, J. A. King and G. M. Odegard, Comparing the Mechanical Response of Di-, Tri-, and Tetra-functional Resin Epoxies with Reactive Molecular Dynamics, *J. Polym. Sci., Part B: Polym. Phys.*, 2018, **56**(3), 255–264.

64 G. M. Odegard, B. D. Jensen, S. Gowtham, J. Wu, J. He and Z. Zhang, Predicting mechanical response of crosslinked epoxy using ReaxFF, *Chem. Phys. Lett.*, 2014, **591**, 175–178.

65 Q. Lu, M. Arroyo and R. Huang, Elastic bending modulus of monolayer graphene, *J. Phys. D: Appl. Phys.*, 2009, **42**(10), 102002.